nature climate change

ARTICLES
https://doi.org/10.1038/s41558-020-0892-z

Extremes become routine in an emerging new Arctic

Laura Landrum ✉ and Marika M. Holland

The Arctic is rapidly warming and experiencing tremendous changes in sea ice, ocean and terrestrial regions. Lack of long-term scientific observations makes it difficult to assess whether Arctic changes statistically represent a 'new Arctic' climate. Here we use five Coupled Model Intercomparison Project 5 class Earth system model large ensembles to show how the Arctic is transitioning from a dominantly frozen state and to quantify the nature and timing of an emerging new Arctic climate in sea ice, air temperatures and precipitation phase (rain versus snow). Our results suggest that Arctic climate has already emerged in sea ice. Air temperatures will emerge under the representative concentration pathway 8.5 scenario in the early- to mid-twenty-first century, followed by precipitation-phase changes. Despite differences in mean state and forced response, these models show striking similarities in their anthropogenically forced emergence from internal variability in Arctic sea ice, surface temperatures and precipitation-phase changes.

The Arctic is a region of extremes, and Arctic climate is changing at a much rapider pace than at lower latitudes[1–4], with changes occurring across atmosphere, ocean, sea-ice and terrestrial systems. Northern Hemisphere (NH) minimum sea-ice extents (SIEs) have been lower in each of the past 13 years than any other years in the satellite era (1979–present; National Snow and Ice Data Center (NSIDC) monthly sea-ice index[5]). Over the past decade, there have been increasing numbers of extreme warm winter air temperature events linked to decreasing winter sea ice[6–8] and early-season rain-on-snow events with dire ecological consequences[9–12]. While these changes appear extreme compared with the recent past, are they climatic extremes in a statistical sense, or do they represent expected events in a new Arctic climate?

Numerous observational and modelling studies investigate the emergence of new climates, particularly for terrestrial systems and subpolar latitudes (for examples, see refs. [13–18]). While emergence of a new Arctic open-water season has been explored[19], and changes in permafrost, land and sea ice generally synthesized[20], to the best of our knowledge there has not been work that quantifies the timing and nature of the emergence of a new Arctic climate across both ocean and land regions.

Characterizing climate in an era of rapid climate change is problematic for regions such as the Arctic where observational data are relatively short, sparse and primarily from the modern satellite era—a time of dramatic change. The Arctic experienced warming and sea-ice loss in the early twentieth century in magnitudes similar to those of the 1980s[21–23], and recent studies suggest that Atlantic and Pacific multi-decadal variability may have played an important role[21,22]. Characterizing this type of multi-decadal variability in the Arctic is challenging given the short observational records. In addition, systematic biases and disagreement in variabilities in atmospheric data[24,25] and relative sparseness of sea-ice data[23] make it difficult to establish the true temperature and sea-ice variability. Quantifying the distribution of climate events is important for understanding a particular climate state, determining when a statistically different and therefore 'new' climate has emerged and giving insight into possible future extremes of societal and ecological importance. Climate model simulations with large ensemble sets provide a means forward, enabling separation of a forced response from internal variability. Here we use output from the Coupled Model Intercomparison Project 5 (CMIP5) class Multi-Model Large Ensemble (MMLE[26]) Archive to robustly characterize twentieth-century climate and to quantify the emergence of a new Arctic climate in twentieth- and twenty-first-century simulations subject to historical and the 'high warming' representative concentration pathway (RCP) 8.5 forcing scenario.

The Arctic is in part unique because of its frozen state. Thus, we use three key variables that provide information on the transition of the Arctic away from a dominantly frozen state: sea ice, surface air temperature and precipitation phase (rain versus snow). These metrics provide information on both marine and terrestrial systems, are important aspects of changing Arctic seasonality and are properties of the climate relevant for society.

Sea ice

Arctic temperatures are rising much more rapidly than at lower latitudes—a process termed Arctic amplification. Although the relative contributions of different mechanisms to Arctic amplification is an area of active research, near-surface Arctic amplification is strongly influenced by changes in both sea-ice concentrations (SICs, an albedo feedback) and sea-ice thickness (SIT, an insulating feedback)[3,4,27–38]. We begin our investigation with sea ice, and in particular with changes in the extremes of the annual sea-ice cycle—the minimum and maximum SIEs—which currently occur in mid-September and mid-March, respectively.

The observed decadal mean SIE minimum has decreased by 2.4 million km^2 (31%) from the beginning of the satellite era (1979–1988) to present (2009–2018). Although the satellite record is insufficient to determine whether this represents a change in climate outside the bounds of earlier twentieth-century variability, the CMIP5-MMLE suggests that it may. The observational sea-ice record—mean, variability and recent rate of decrease—lie well within the range of these five ensembles (Fig. 1, Table 1, Extended Data Figs. 1 and 2, Supplementary Fig. 1 and Supplementary Discussion). Decadal means for both minimum and maximum observed SIE also lie within internal variability of each individual

National Center for Atmospheric Research, Boulder, CO, USA. ✉e-mail: landrum@ucar.edu

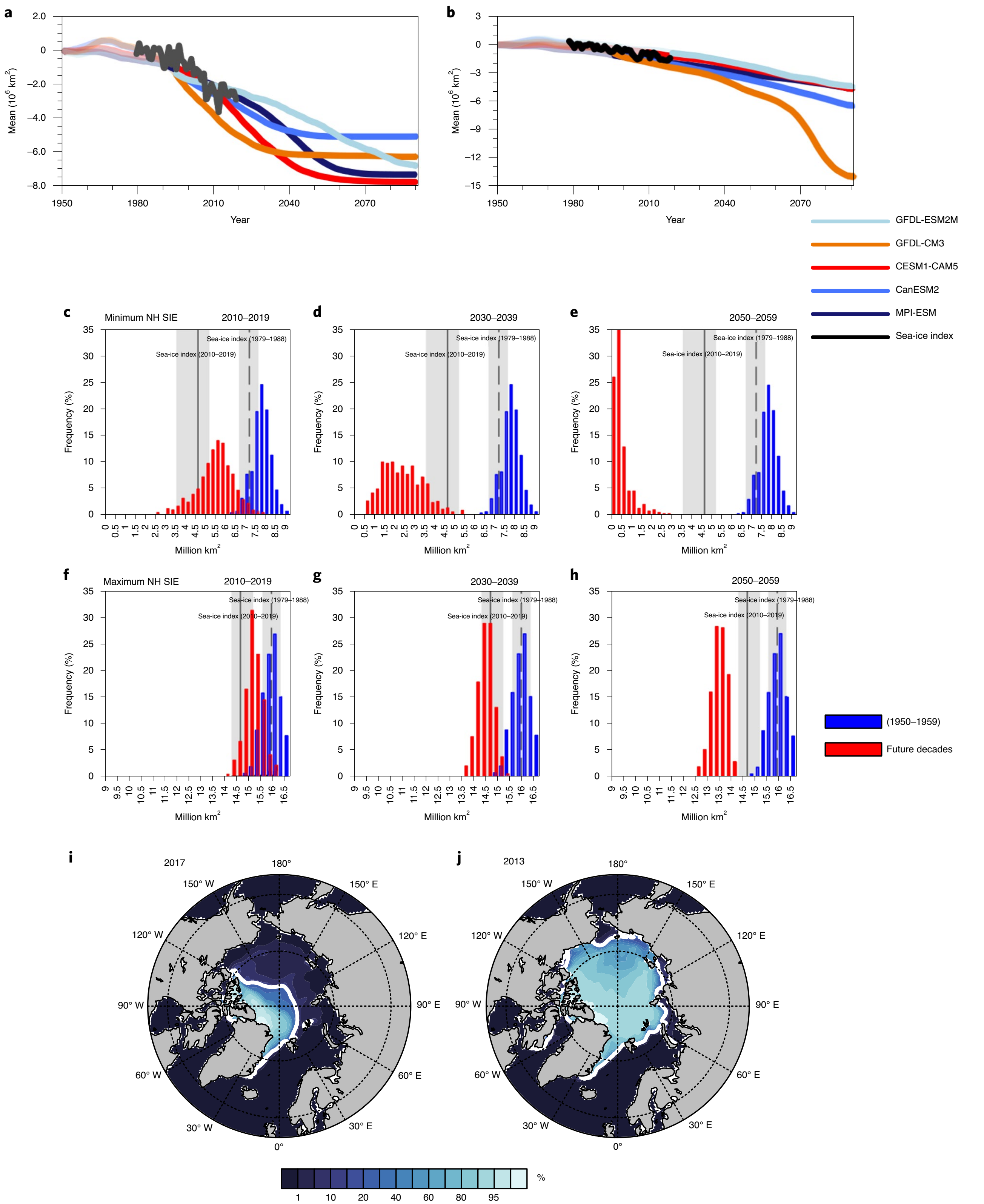

Fig. 1 | Changes in means and distributions of annual minimum and maximum NH SIE. **a**,**b**, Decadal ensemble mean minimum (**a**) and maximum (**b**) NH SIE anomalies for CMIP5-MMLE. Anomalies are computed by subtracting the 1950–1959 ensemble mean from each model. Lines are faded/bright before/after ToE. **c**–**h**, Histograms of CESM1-CAM5 annual minimum (**c**–**e**) and maximum (**f**–**h**) NH SIE in the early twentieth century (1950–1959; blue) and later decades (red): 2010–2019 (**c**,**f**); 2030–2039 (**d**,**g**); 2050–2059 (**e**,**h**). First (1979–1986) and most recent (2010–2019) decadal means from the NSIDC monthly sea-ice index[5] are shown in dashed/solid lines, respectively, with observed range shown in light grey for reference. **i**,**j**, CESM1-CAM5 SICs for smallest (2017) (**i**) and largest (2013) (**j**) NH SIE minimums during 2010–2019. The 15% contour is shown in white. Monthly SICs are used for all calculations.

Table 1 | CMIP5-MMLE characteristics, mean SIEs and changes in mean summer SIEs, and ToE for three metrics (SIEs, surface temperatures and precipitation phase)

		SIE				ToE							Reference
		1950–1959 mean (s.d.) ($\times 10^6$ km^2)		First ice-free (<1×10^6 km^2) decadal mean	(2009–2018) – (1979–1988) min	SIE		70°–90° N					
								Surface temperature		Rain days			
Model	No. of members	Min	Max			Min	Max	Oct	Feb	First	Last	Duration	
CanESM2	50	5.12 (0.65)	15.78 (0.53)	2030	−2.56	1996	2000	2033	2049	2068	2048	2042	68
CESM1-CAM5	40	7.85 (0.46)	15.99 (0.53)	2042	−1.93	1995	2010	2027	2046	2071	2052	2047	69
GFDL-CM3	20	6.32 (0.66)	15.16 (0.43)	2023	−3.82	1995	1997	2018	2032				70
GFDL-ESM2M	30	7.29 (0.65)	18.91 (0.42)	2079	−1.57	1995	2020	2044	2065				71
MPI-ESM	99	7.39 (0.46)	15.67 (0.54)	2052	−1.42	1992	1997	2032	2052				72
NSIDC sea-ice index 1979–1988 mean	1	7.05	16.34		−2.40								5

ensemble, with the exception of the anaemic minimum SIE of the CanESM and the excessive maximum SIE of the GFDL-ESM2M. However, the most recent observed decadal mean minimum SIE (4.7 million km^2, 2009–2018) lies outside or nearly outside the simulated (1980–1989) spread for all of the ensembles except the CanESM, which has the lowest mean sea ice of the models. The current minimum SIE may indeed be statistically 'new' compared with not only the mid-twentieth century but also the beginning of the satellite era.

By the 2010s, the CMIP5-MMLE minimum SIE histograms have noticeably shifted—showing both a lower mean and a larger spread, with only a few of the largest minimum SIEs overlapping with the smallest ones from the reference 1950 decade (Fig. 1 and Supplementary Fig. 1). Variability in the minimum SIE increases in the early twenty-first century and then decreases as more ensemble members become ice free (<1 million km^2) in each of the ensembles (and documented for individual models in previous work, for example, refs. [39–41]). Distributions in the minimum and maximum SIEs continue to diverge from the reference period, with complete separation of the distributions in both minimum and maximum NH SIE in the first half of the twenty-first century in all ensembles except the one that has the most extensive SIE (GFDL-ESM2M). These results are similar to previous observational work indicating that the Arctic ice regime became more seasonal in the 2010s[15].

To give a sense for the tremendous regional variability that the spread in minimum SIE implies, we show SICs from two representative ensemble members from one model (CESM1-CAM5) exhibiting the smallest and largest minimum SIEs during the 2010s (Fig. 1). The enormous differences in geographical ranges of SIC foretell of potentially large risk management challenges within the context of navigation, habitat, coastal access and erosion, among others.

To address our question of when the Arctic climate becomes significantly different from that of the mid-twentieth century, we define a time of emergence (ToE) as the year when the decadal mean from each ensemble exceeds the reference 1950 decade by 2 s.d. on the basis of the reference decade variability. With this definition, the annual minimum and annual maximum NH SIE emerge across the different models in 1992–1996 and 1997–2020 (where the year refers to the first year of the decadal mean), respectively (Table 1). More specifically, while our ToE uses a reference 1950 climate, we find that the annual minimum (maximum) SIEs emerge also from the 1980 climate within 15–24 (16–38) years across the CMIP5-MMLE (not shown). ToE for maximum SIEs lag those for the minimum SIEs in each model ensemble, yet still emerge by 2020, before differences in RCP forcing scenarios are sizable[42]. These results are largely consistent with comparisons with the extended sea-ice data, which begins in 1850 (ref. [23]), although caution should be used in comparing with this dataset due to large gaps in areal coverage (Supplementary Information).

'Ice-free' Arctic is generally defined as when SIE falls below 1 million km^2. At extents below this, the only remaining sea ice lies in the Canadian Archipelago—a region of thick sea ice that is particularly difficult to melt[43]. Under the RCP 8.5 scenario, CMIP5-MMLE simulated decadal mean minimum SIEs fall below the ice-free criteria as early as 2023 and as late as 2079 (Table 1)—a much larger spread than for the SIE ToEs, and related not only to different model physics but also to mean sea ice at the beginning of the twenty-first century (for example, refs. [44–46]). By the end of the twenty-first century, the NH monthly minimum SIE falls below the standard ice-free definition for 3–10 months in all models except the GFDL-ESM2M. In these four models, the mean decadal SIE is 0 with no ice left even in the Canadian Archipelago from August to October or longer (see also ref. [19]). These extreme conditions are found under the RCP 8.5 scenario, and limiting future warming to 1.5 °C could have substantial impacts on September SIE, with notably more summer sea ice present at the end of the twenty-first century[47–49].

Surface air temperatures

Arctic sea-ice conditions in turn influence fall–winter atmospheric conditions[31,50–53]. During the summer, sea ice reflects most incoming solar radiation due to high albedos. Radiation not reflected from the surface can contribute to melting ice and warming the ocean. With reduced sea ice, albedo decreases and the surface ocean is warmed. This heat is subsequently released back to the atmosphere in the fall, delaying the onset of sea-ice growth. During the Arctic winter, sea ice acts as an insulator between the relatively warm ocean and overlying cold atmosphere. There is no solar radiation during the polar night; hence, albedos play no direct role in surface heat budgets. Instead, winter temperatures at the air–sea ice interface are influenced by heat conduction through the sea ice, which is inversely related to SIT[54]. It is important to note that the winter SIT is affected by the summer sea-ice and ocean conditions and onset of ice growth in the fall. In this way, changes in the summer, when maximum SIC losses and albedo changes occur, can indirectly influence winter surface air temperatures.

Currently, observed Arctic amplification is largest in autumn and is related to diminishing summer sea ice[4,27,36]. Climate models suggest that Arctic amplification will become as great, or greater, in the winter months[55–57]. Because of this, we consider the emergence of surface air temperatures by calculating ToE and changes in both

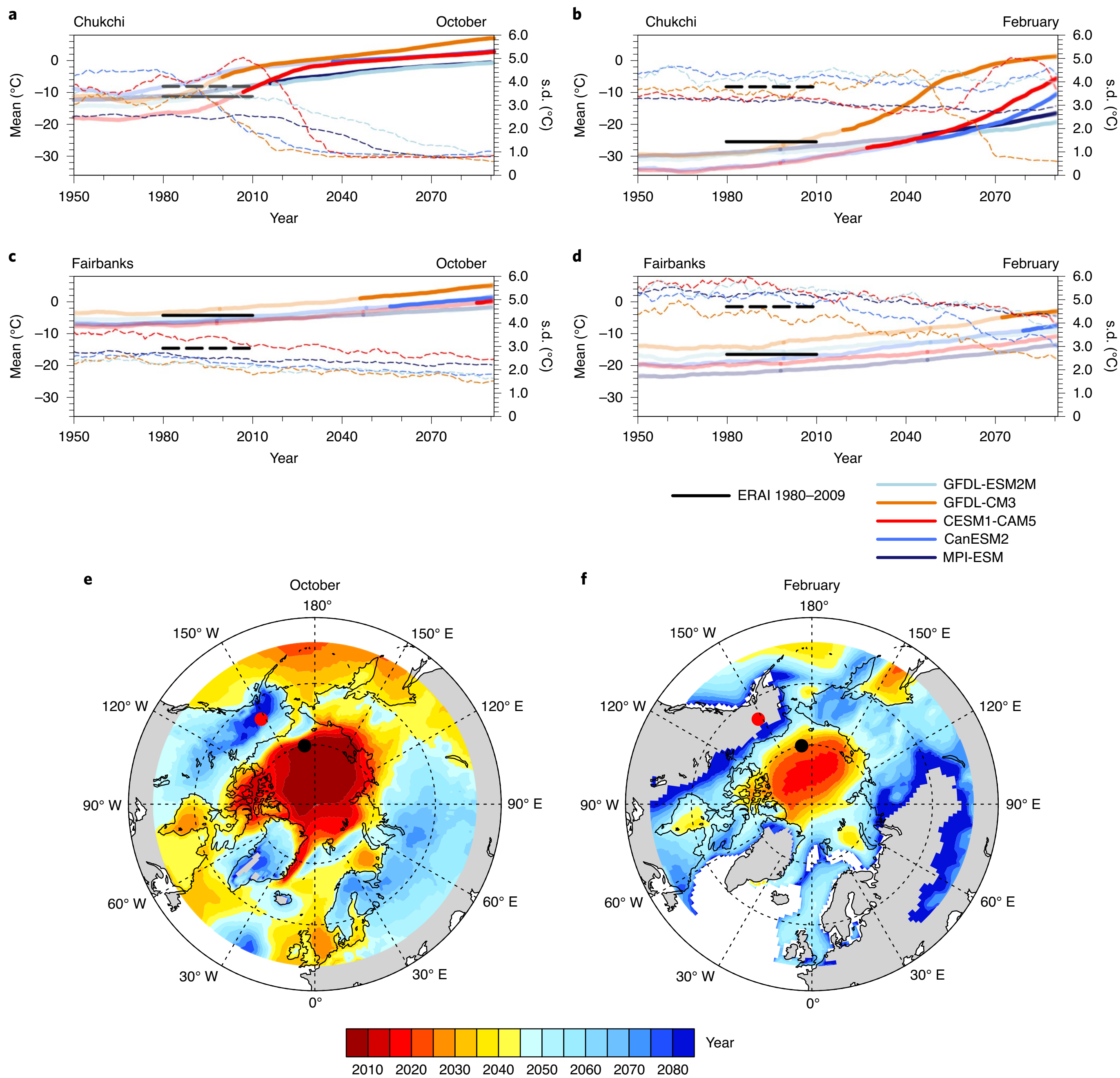

Fig. 2 | Mean October and February surface temperatures and ToE. a–d, CMIP5-MMLE decadal ensemble monthly surface air temperature means (solid lines, left axis) and standard deviations (dashed lines, right axis) for October (**a**,**c**) and February (**b**,**d**) for example ocean (Chukchi Sea, **a**,**b**) and land (Fairbanks, Alaska, **c**,**d**) gridpoints. Mean lines are faded/bright before/after ToE. Black solid/dashed lines show the 1980–2009 ERA-I mean/standard deviation[58]. **e**,**f**, ToE for CESM1-CAM5 surface air temperatures in October (**e**) and February (**f**). Chukchi Sea/Fairbanks, Alaska, locations are shown by black/red dots.

mean and variability for monthly autumn (October) and winter (February) surface temperatures, and we relate these to changes in summer SIC and winter SIT.

October surface air temperatures in the CMIP5-MMLE emerge earliest–in the first half of the twenty-first century—over the Arctic Ocean (Fig. 2 and Extended Data Fig. 3). Winter Arctic Ocean temperatures lag those of fall, emerging in the mid-twenty-first century (Table 1). The land/sea discrepancy in ToE occurs because Arctic Ocean temperatures experience greater warming and have lower variabilities than those of high-latitude land, a result that is also seen in previous work[13]. This is illustrated by time series of mean and standard deviations of October and February monthly temperatures for representative land (Fairbanks, Alaska) and ocean (Chukchi Sea) model gridpoints (Fig. 2). Mean land temperatures warm substantially by the end of the twenty-first century (5–12 °C), yet not nearly as much as over the Arctic Ocean (12–28 °C; Extended Data Figs. 4 and 5). The CMIP5-MMLE temperatures compare reasonably well to the ERA-Interim reanalysis data[58] during the satellite era (Fig. 2).

Associated with polar amplification is a decrease in latitudinal temperature gradient. By the end of the twenty-first century in

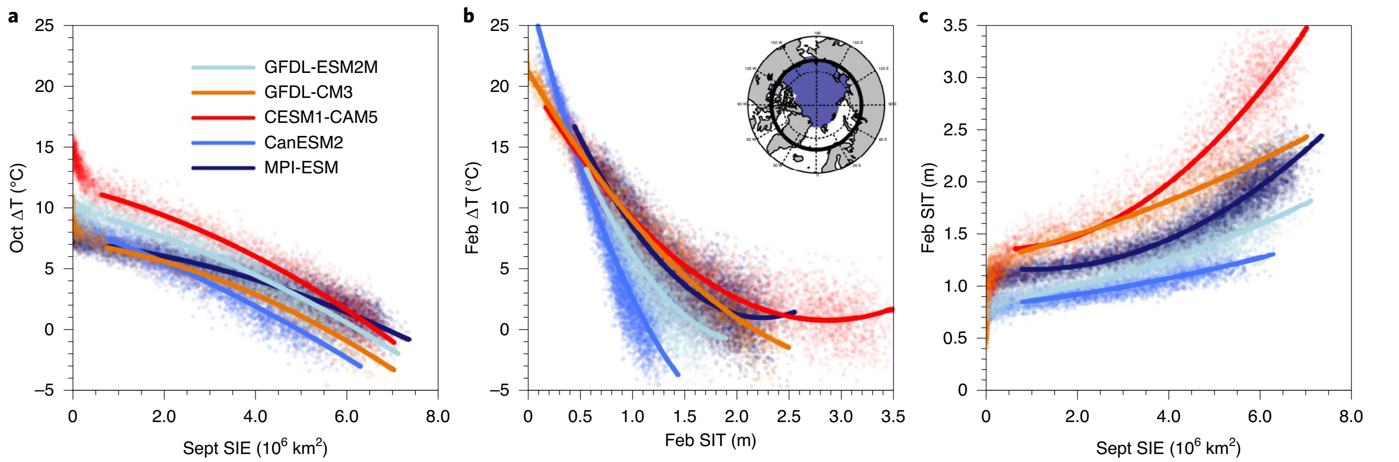

Fig. 3 | Relationships among Arctic Ocean SIEs, SIT and October and February polar (70°–90° N) surface air temperature changes, 1980–2099. **a**–**c**, Changes (from 1950 to 1959) in October monthly temperatures versus mean September SIE (**a**), changes in February surface temperatures versus mean February SIT (**b**) and mean February SIT versus mean September SIE (**c**) for CMIP5-MMLE. Dots represent one simulation, one year. Solid lines are a polynomial fit (excluding ice-free data points). Map inset in **b** shows Arctic Ocean region. Arctic Ocean sea-ice region is the shaded area in the map inset; high-latitude temperature region (70°–90° N) is indicated by the black circle on the map.

all of the CMIP5-MMLE, differences in monthly October mean temperatures between the Chukchi Sea (75° N) and lower-latitude Fairbanks (~65° N) have shrunk substantially (Fig. 2). Rapid warming rates over the Arctic Ocean in the fall precede those in the winter in all CMIP5-MMLE (Fig. 2 and Extended Data Figs. 4 and 5). Furthermore, by the end of the twenty-first century, three out of five of the ensembles simulate greater high-latitude (70°–90° N) winter warming than fall (Supplementary Table 1). Monthly temperature variability is non-stationary: standard deviations decrease dramatically over ice-free ocean areas (October) and near the sea-ice edge (February), highlighting the role of the ocean (with large heat capacity) in modulating surface temperatures. Variability over high-latitude continental regions decreases as well—albeit less than over oceanic regions—probably due to greater warming of cold than warm days, decreasing temperature gradients and resulting changes in meridional heat transport[57,59]. This suggests that changes in extremes in fall–winter temperatures will be due primarily to shifts in the mean with lower variability as the Arctic Ocean transitions from sea-ice- to open-water-dominated summers and from relatively thick to relatively thin winter sea ice.

Late-summer SIEs in the Arctic Ocean influence both high-latitude October surface temperature changes and winter SIT as newly exposed and warmed ocean releases heat back to the atmosphere in fall (Fig. 3). February temperatures are closely related to the winter SIT, particularly where the mean ice thickness falls below 2 m, in all CMIP5-MMLE. Winter SIE declines steadily (albeit more slowly than summer SIE) throughout the twenty-first century. The central Arctic basin is still ice covered by 2100 in four of the CMIP5-MMLE (Extended Data Figs. 1 and 5), yet surface temperatures show marked winter warming even over the ice pack as the ice thins. The CESM1-CAM5—which saves ice concentrations by thickness category—gives an example of dramatic thickness changes: in 1980, thin ice (less than 0.64 m thick) is largely confined to the outer edges of the ice pack. By the end of the twenty-first century under the RCP 8.5 scenario, the thin-ice concentration has increased by over 40% in the central Arctic basin. Similarly, as the ice pack thins, ice 0.64–1.39 m thick increases in the central Arctic until mid-twenty-first century and then decreases as the thinnest ice becomes dominant. These changes in ice thickness lead to large changes in conductive heat flux from the underlying relatively warmer ocean through the ice to the atmosphere and to strong relationships between winter ice thickness and winter surface warming in all of the CMIP5-MMLE.

Precipitation phase

Concurrent with surface temperature changes are changes in the seasonal cycle of precipitation phase (rain versus snow; for example, refs. [60,61]). Precipitation phase has enormous implications for energy budgets, hydrological cycles and management, and ecology (for example, refs. [11,62–65] and references therein). We explore changes in precipitation phase in the two CMIP5-MMLE models (CESM1-CAM5 and CanESM2) that have daily solid and liquid precipitation data available. This includes analysis of the timing of the snow-to-rain transition and the duration of the rainy season. Precipitation-phase changes in both models respond similarly, simulating late twentieth-century first- and last-rain-day changes within the range of observations[66] and ocean areas with greater relative changes than land areas (Fig. 4 and Extended Data Figs. 6–8).

Consistent with October surface temperatures, Arctic ocean areas show both larger changes and earlier ToEs in the last rain day than do land areas (Fig. 4 and Extended Data Fig. 7). First-rain-day changes resemble those of winter (February) temperature changes. Changes to first and last rain days influence the rain-season length, and although increases in the rain-season duration are most dramatic over the Arctic ocean, continental regions see increases by 20–60 days by the mid-twenty-first century, and by the end of the twenty-first century, increases of 60–90+ days in rain-season length occur nearly everywhere (except areas of Siberia with increases of 30–60 days; Extended Data Fig. 8). By the end of the twenty-first century under the RCP 8.5 scenario, there are regions where rain can occur any month of the year, with first and last days of rain occurring within one standard deviation of each other (for example, Fig. 4), with enormous consequences for ecosystems, water resource management, flood planning and infrastructure[67].

Conclusions

Has a new Arctic emerged? And if not, will it do so within this century? We have addressed these questions by assessing three different metrics of the Arctic climate from five CMIP5-class multi-model large ensembles subject to the RCP 8.5 forcing scenario. These metrics—sea ice, air temperature and precipitation phase—represent different aspects of the frozen state of the Arctic. On the basis of

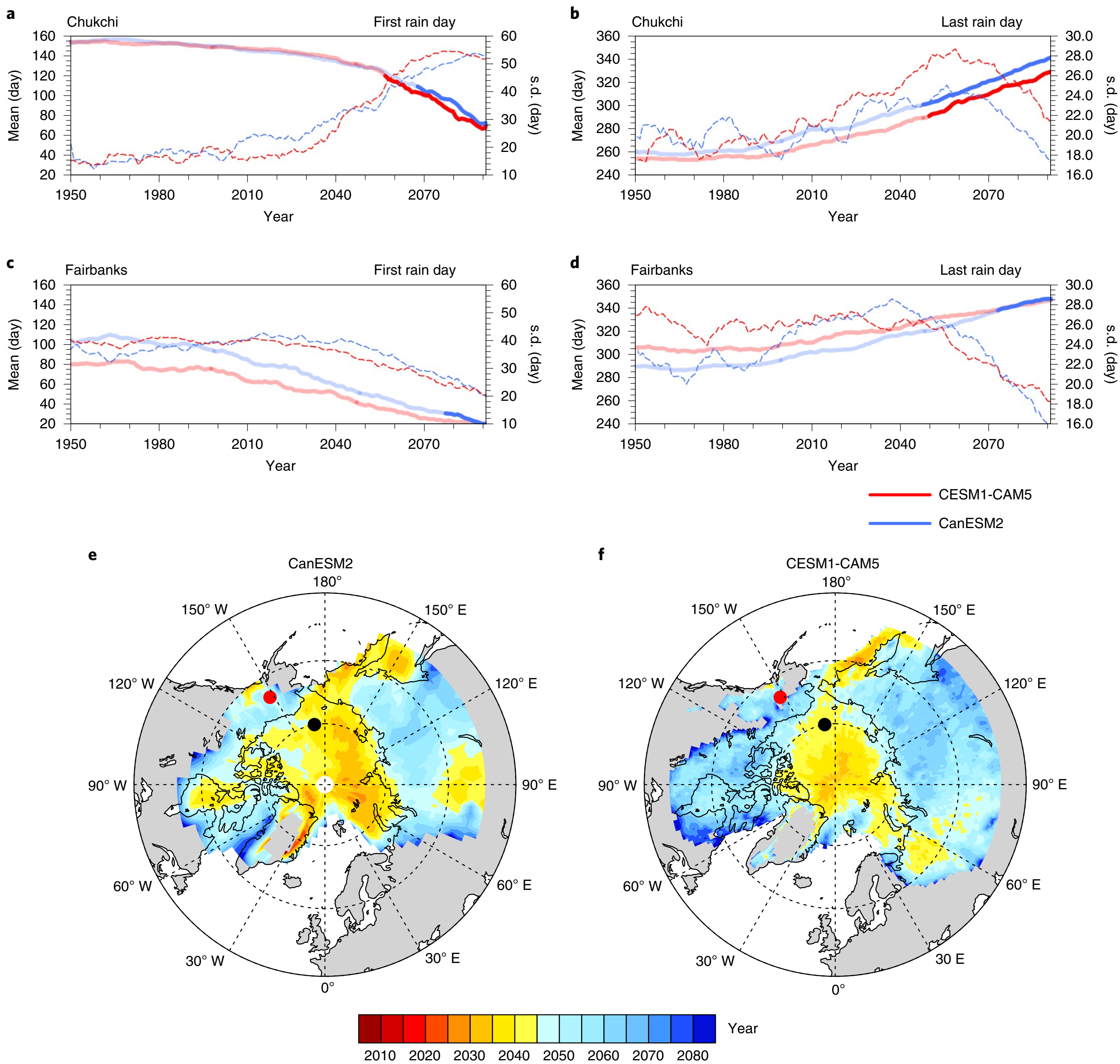

Fig. 4 | Mean first- and last-rain-day changes and ToE of the rain-season duration. a–d, CMIP5-MMLE decadal ensemble mean (solid lines, left axis) and standard deviations (dashed lines, right axis) for first rain day (**a**,**c**) and last rain day (**b**,**d**) for example ocean (Chukchi Sea, **a**,**b**) and land (Fairbanks, Alaska, **c**,**d**) gridpoints. Mean lines are faded/bright before/after time of emergence. **e**,**f**, ToE for CanESM2 (**e**) and CESM1-CAM5 (**f**) rain-season length. Chukchi Sea/Fairbanks, Alaska, locations are shown by black/red dots.

our definition of ToE, sea-ice climate emerges first in the late twentieth to early twenty-first century, surface air temperatures emerge second in the early to mid-twenty-first century, and seasonal precipitation-phase change emerges last in the mid-twenty-first century. By 2100, a new Arctic has emerged in all of these properties. Despite differences in mean state and forced response, the CMIP5-MMLE show striking similarities in their anthropogenically forced emergence from internal variability in Arctic sea ice, surface temperatures and precipitation-phase changes.

These changes are interrelated. Rapid changes in SIC and SIT contribute to extreme changes in first fall (October) then winter (February) surface air temperatures. Winter warming is greatest over the Arctic Ocean in the last half of the twenty-first century when ensemble mean February sea ice has thinned (four of the models) or become ice free (one model). Surface temperatures in turn influence the phase of precipitation (rain versus snow), with fall temperatures and last rain days emerging before winter temperatures and first rain days. The nearly identical nature of SIE histograms (both minimum and maximum) between 1950 and 1980 indicate that the rapid climatic change in all of the CMIP5-MMLE begins at the end of the twentieth century, after the beginning of the satellite era (1979)—suggesting that the satellite record of sea ice occurs during a period of tremendous environmental change and does not statistically represent a base 'climate' from which the Arctic is changing.

Taken together, this work suggests that the Arctic is already transitioning from a cryosphere-dominated system. Changes in sea ice at the end of the twentieth century are substantial, and if emissions follow an RCP 8.5-like path, this region is likely to experience extremes in temperature, sea ice and precipitation phase far outside anything experienced in the past century and probably much longer. All five CMIP5-MMLE simulate mean ice-free summer by 2100, and three of these ensemble projections (the three with the closest ice extents to the observations during the satellite era) suggest that the Arctic will remain completely ice free for 3–4 months. Not only will the warming exceed that of lower latitudes, but daily fall–winter temperatures will increase by 16–28 °C for most of the Arctic Ocean. Rainfall will replace snowfall, with an extension of the rainy season by 2–4 months. These changes have extreme consequences for Arctic communities and local ecosystems. Notably, reductions in GHGs can change this trajectory and may postpone or even avoid the emergence of a new Arctic in many climate properties (for example, ref. [47]).

Online content

Any methods, additional references, Nature Research reporting summaries, source data, extended data, supplementary information, acknowledgements, peer review information; details of author contributions and competing interests; and statements of data and code availability are available at https://doi.org/10.1038/s41558-020-0892-z.

Received: 4 October 2019; Accepted: 31 July 2020;
Published online: 14 September 2020

References

1. Box, J. E. et al. Key indicators of Arctic climate change: 1971–2017. *Environ. Res. Lett.* **14**, 045010 (2017).
2. Hansen, J., Ruedy, R., Sato, M. & Lo, K. Global surface temperature change. *Rev. Geophys.* **48**, RG4004 (2010).
3. Serreze, M. C. & Barry, R. G. Processes and impacts of Arctic amplification: a research synthesis. *Glob. Planet. Change* **77**, 85–96 (2011).
4. Screen, J. A. & Simmonds, I. I. The central role of diminishing sea ice in recent Arctic temperature amplification. *Nature* **464**, 1334–1337 (2010).
5. Fetterer, F., Knowles, K., Meier, W. N., Savoie, M. & Windnagel, A. K. *Sea Ice Index, Version 3* (Northern Hemisphere monthly) (NSIDC, accessed 22 April 2020); https://doi.org/10.7265/N5K072F8
6. Graham, R. et al. Increasing frequency and duration of Arctic winter warming events. *Geophys. Res. Lett.* **44**, 6974–6983 (2017).
7. Moore, G. W. K. The December 2015 North Pole warming event and the increasing occurrence of such events. *Nat. Sci. Rep.* **6**, 39084 (2016).
8. Rinke, A. et al. Extreme cyclone events in the Arctic: Wintertime variability and trends. *Environ. Res. Lett.* **12**, 094006 (2017).
9. Cohen, J., H. Ye, H. & Jones, J. Trends and variability in rain-on-snow events. *Geophys. Res. Lett.* **42**, 7115–7122 (2015).
10. Hansen, B. B., Aanes, R., Herfindal, I., Kohler, J. & Sæther, B.-E. Climate, icing, and wild Arctic reindeer: past relationships and future prospects. *Ecology* **92**, 1917–1923 (2011).
11. Rennert, K., Roe, G., Putkonen, J. & Bitz, C. M. Soil thermal and ecological impacts of rain on snow events in the circumpolar Arctic. *J. Clim.* **22**, 2302–2315 (2008).
12. Stien, A. et al. Congruent responses to weather variability in high Arctic herbivores. *Biol. Lett.* **8**, 1002–1005 (2012).
13. Beaumont, L. J. et al. Impacts of climate change on the world's most exceptional ecoregions. *Proc. Natl Acad. Sci. USA* **108**, 2306–2311 (2011).
14. Giorgi, F. & Bi, X. Time of emergence (TOE) of GHG forced precipitation change hot-spots. *Geophys. Res. Lett.* **36**, L06709 (2009).
15. Haine, T. W. & Martin, T. The Arctic–Subarctic sea ice system is entering a seasonal regime: implications for future Arctic amplification. *Sci. Rep.* **7**, 4618 (2017).
16. King, A. D. et al. The timing of anthropogenic emergence in simulated climate extremes. *Environ. Res. Lett.* **10**, 094015 (2015).
17. Lehner, F., Deser, C. & Terray, L. Toward a new estimate of "time of emergence" of anthropogenic warming: insights from dynamical adjustment and a large initial-condition model ensemble. *J. Clim.* **30**, 7739–7756 (2017).
18. Mahlstein, I., Heger, G. & Solomon, S. Emerging local warming signals in observational data. *Geophys. Res. Lett.* **39**, L21711 (2012).
19. Barnhart, K. R., Miller, C. R., Overeem, I. & Kay, J. E. Mapping the future expansion of Arctic open water. *Nat. Clim. Change* **6**, 280–285 (2016).
20. Moon, T. A. et al. The expanding footprint of rapid Arctic change. *Earths Future* **7**, 212–218 (2019).
21. Hegerl, G. C., Brönnimann, S., Schurer, A. & Cowan, T. The early 20th century warming: anomalies, causes, and consequences. *Wiley Interdiscip. Rev. Clim. Change* **9**, e522 (2018).
22. Tokinaga, H., Xie, S. P. & Mukougawa, H. Early 20th-century Arctic warming intensified by Pacific and Atlantic multidecadal variability. *Proc. Natl Acad. Sci. USA* **114**, 6227–6232 (2017).
23. Walsh, J. E., Fetterer, F., Stewart, J. Scott & Chapman, W. L. A database for depicting Arctic sea ice variations back to 1850. *Geographical Rev.* **107**, 89–107 (2016).
24. Brönnimann, S. et al. A multi-data set comparison of the vertical structure of temperature variability and change over the Arctic during the past 100 years. *Clim. Dyn.* **39**, 1577–1598 (2012).
25. Cowtan, K. & Way, R. G. Coverage bias in the HadCRUT4 temperature series and its impact on recent temperature trends. *Q. J. R. Meteorol. Soc.* **140**, 1935–1944 (2014).
26. Deser, C. et al. Insights from Earth system model initial-condition large ensembles and future prospects. *Nat. Clim. Change* https://doi.org/10.1038/s41558-020-0731-2 (2020).
27. Dai, A., Luo, D., Song, M. & Liu, J. Arctic amplification is caused by sea-ice loss under increasing CO_2. *Nat. Commun.* **10**, 121 (2019).
28. Hall, A. The role of surface albedo feedback in climate. *J. Clim.* **17**, 1550–1568 (2004).
29. Holland, M. M. & Bitz, C. M. Polar amplification of climate change in coupled models. *Clim. Dyn.* **21**, 221–232 (2003).
30. Kumar, A. et al. Contribution of sea ice loss to Arctic amplification. *Geophys. Res. Lett.* https://doi.org/10.1029/2010GL045022 (2010).
31. Labe, Z. M., Peings, Y. & Magnusdottir, G. Contributions of ice thickness to the atmospheric response from projected Arctic sea ice loss. *Geophys. Res. Lett.* https://doi.org/10.1029/2018GL078158 (2018).
32. Lang, A., Yang, S. & Kaas, E. Sea ice thickness and recent Arctic warming. *Geophys. Res. Lett.* **44**, 409–418 (2017).
33. Pithan, F. & Mauritsen, T. Arctic amplification dominated by temperature feedbacks in contemporary climate models. *Nat. Geosci.* **7**, 181–184 (2014).
34. Screen, J. A., Simmonds, I., Deser, C. & Tomas, R. The atmospheric response to three decades of observed Arctic sea ice loss. *J. Clim.* **26**, 1230–1248 (2013).
35. Screen, J. A. et al. Consistency and discrepancy in the atmospheric response to Arctic sea-ice loss across climate models. *Nat. Geosci.* **11**, 155–163 (2018).
36. Serreze, M. C., Barrett, A. P., Stroeve, J. C., Kindig, D. N. & Holland, M. M. The emergence of surface-based Arctic amplification. *Cryosphere* **3**, 11–19 (2009).
37. Smith, D. M. et al. The Polar Amplification Model Intercomparison Project (PAMIP) contribution to CMIP6: investigating the causes and consequences of polar amplification. *Geosci. Model Dev.* **12**, 1139–1164 (2019).
38. Sun, L. et al. Drivers of 2016 record Arctic warmth assessed using climate simulations subjected to factual and counterfactual forcing. *Weather Clim. Extrem.* https://doi.org/10.1016/j.wace.2017.11.001 (2018).
39. Holland, M. M., Bitz, C. M., Tremblay, B. & Bailey, D. A. in *Arctic Sea Ice Decline: Observations, Projections, Mechanisms, and Implications* (eds DeWeaver, E. T. et al.) 133–150 (AGU, 2008).
40. Goosse, H., Arzel, O., Bitz, C. M., de Montety, A. & Vancoppenolle, M. Increased variability of the Arctic summer ice extent in a warmer climate. *Geophys. Res. Lett.* **36**, L23702 (2009).
41. Mioduszewski, J., Vavrus, S., Wang, M., Holland, M. & Landrum, L. Future interannual variability of Arctic sea ice in coupled climate models. *Cryosphere* **13**, 113–124 (2018).
42. Meinshausen, M. et al. The RCP greenhouse gas concentrations and their extension from 1765 to 2300. *Climatic Change* **109**, 213–241 (2011).
43. Liu, J., Song, M., Horton, R. M. & Hu, Y. Reducing spread in projected ice-free Arctic. *Proc. Natl Acad. Sci. USA* https://doi.org/10.1073/pnas.1219716110 (2013).
44. Massonnet, F. et al. Constraining projections of summer Arctic sea ice. *Cryosphere Discuss.* **6**, 2931–2959 (2012).
45. Overland, J. E. & Wang, M. When will the summer Arctic be nearly sea ice free. *Geophys. Res. Lett.* **40**, 2097–2101 (2013).
46. Wang, M. & Overland, J. E. Projected future duration of the sea-ice-free season in the Alaskan Arctic. *Prog. Oceanogr.* **136**, 50–59 (2015).
47. Jahn, A. Reduced probability of ice-free summers for 1.5 °C compared to 2 °C warming. *Nat. Clim. Change* **8**, 409–413 (2018).
48. Screen, J. A. & Williamson, D. Ice-free Arctic at 1.5 °C? *Nat. Clim. Change* **7**, 230–231 (2017).
49. Sigmond, M., Fyfe, J. C. & Swart, N. C. Ice-free Arctic projections under the Paris Agreement. *Nat. Clim. Change* **8**, 404–408 (2018).

50. Blüthgen, J., R. Gerdes, R. & Werner, M. Atmospheric response to the extreme Arctic sea ice conditions in 2007. *Geophys. Res. Lett*. https://doi.org/10.1029/2011GL050486 (2012).
51. Francis, J. A., Chan, W., Leathers, D. J., Miller, J. R. & Veron, D. Winter Northern Hemisphere weather patterns remember summer Arctic sea-ice extent. *Geophys. Res. Lett.* **36**, L07503 (2009).
52. Francis, J. A. & Vavrus, S. J. Evidence linking Arctic amplification to extreme weather in mid-latitudes. *Geophys. Res. Lett.* **39**, LO6801 (2012).
53. Jaiser R., Dethloff, K., Handorf, D., Rinke, A. & Cohen, J. Impact of sea ice cover changes on the Northern Hemisphere atmospheric winter circulation. *Tellus A* https://doi.org/10.3402/tellusa.v64i0.11595 (2012).
54. Maykut, G. A. & Untersteiner, N. Some results from a time-dependent thermodynamic model of sea ice. *J. Geophys. Res.* **76**, 1550–1575 (1972).
55. Deser, C., Tomas, R., Alexander, M. & Lawrence, D. The seasonal atmospheric response to projected Arctic sea ice loss in the late 21st century. *J. Clim.* **23**, 333–351 (2010).
56. Bintanja, R. & van der Linden, E. C. The changing seasonal climate in the Arctic. *Sci. Rep*. https://doi.org/10.1038/srep01556 (2012).
57. Screen, J. A. Arctic amplification decreases temperature variance in northern mid- to high-latitudes. *Nat. Clim. Change* **4**, 577–582 (2014).
58. Dee, D. P. et al. The ERA-Interim reanalysis: configuration and performance of the data assimilation system. *Q. J. R. Meteorol. Soc.* **137**, 553–597 (2011).
59. Rhines, A., McKinnon, K. A., Tingley, M. P. & Huybers, P. Seasonally resolved distributional trends of North American temperatures show contraction of winter variability. *J. Clim.* **30**, 1139–1157 (2017).
60. Pan, C. G., Kirchner P. B., Kimball, J. S., Kim, Y. & Du, J. Rain-on-snow events in Alaska, their frequency and distribution from satellite observations. *Environ. Res. Lett*. https://doi.org/10.1088/1748-9326/aac9d3 (2018).
61. Ye, H. Changes in frequency of precipitation types associated with surface air temperature over northern Eurasia during 1936–90. *J. Clim.* **29**, 729–734 (2008).
62. Callaghan, T. V. et al. Multiple effects on changes in Arctic snow cover. *Ambio* **40**, 32–45 (2011).
63. Conway, H. & Raymond, C. F. Snow stability during rain. *J. Glaciol.* **39**, 635–642 (1993).
64. McCabe, G. J., Clark, M. P. & Hay, L. E. Rain-on-snow events in the western United States. *Bull. Am. Meteorol. Soc.* **88**, 319–328 (2007).
65. Putkonen, J. & G. Roe, G. Rain-on-snow events impact soil temperatures and affect ungulate survival. *Geophys. Res. Lett.* **30**, 1188 (2003).
66. Ye, H. & Cohen, J. Shorter snowfall season associated with higher air temperatures over northern Eurasia. *Environ. Res. Lett.* **8**, 014052 (2013).
67. Hansen, B. B. et al. Warmer and wetter winters: characteristics and implications of an extreme weather event in the high Arctic. *Environ. Res. Lett.* **9**, 114021 (2014).
68. Kirchmeier-Young, M. C., Zwiers, F. W. & Gillett, N. P. Attribution of extreme events in Arctic sea ice extent. *J. Clim.* **30**, 553–571 (2017).
69. Kay, J. E. et al. The Community Earth System Model (CESM) Large Ensemble project: a community resource for studying climate change in the presence of internal climate variability. *Bull. Am. Meteorol. Soc.* **96**, 1333–1349 (2015).
70. Sun, L., Alexander, M. & Deser, C. Evolution of the global coupled climate response to Arctic sea ice loss during 1990–2090 and its contribution to climate change. *J. Clim.* **31**, 7823–7843 (2018).
71. Rodgers, K. B., Lin, J. & Frölicher, T. L. Emergence of multiple ocean ecosystem drivers in a large ensemble suite with an Earth system model. *Biogeosciences* **12**, 3301–3320 (2015).
72. Maher, N. et al. The max planck institute grand ensemble—enabling the exploration of climate system variability. *J. Adv. Model. Earth Syst.* **11**, 2050–2069 (2019).

Methods

The CMIP5-MMLE. To statistically describe Arctic climate we use model output for five CMIP5-class large ensemble datasets obtained through the MMLE Archive (MMLEA)[26]. The initial years for the CMIP5-MMLE range from 1850 to 1950, and therefore the earliest decade for which we had data from all models defines our base climate (1950–1959). The CMIP5-MMLE are forced with historical forcing until 2005 and then RCP 8.5 forcing from 2005 to 2100 (the no-mitigation scenario with a top of the atmosphere radiative forcing of 8.5 W m^{-2} by 2100). The CMIP5-MMLE simulations represent different realizations under identical forcing with different models and allow us to assess both simulated internal climate variability and differences due to different model structures. Whereas 30 years is often used to characterize 'climate' (for example, ref. [73]), with 20–99 ensemble members, climate can be determined using much shorter periods. This allows for statistical description of climate on decadal (or shorter) periods. Annual simulated values, for example, will give 200–990 instances per decadal period.

SIC and SIT data. The MMLEA includes data from seven models—six of which include monthly sea-ice data. We used the five models that meet one (CanESM2, GFDL-CSM and GFDL-ESM2M) or both (CESM1-CAM5, MPI) of the criteria of Wang and Overland[46] for study of Arctic sea ice, namely, that the modelled amplitude of the seasonal cycle and the monthly SIE fall within 20% of the observations. We did not include CSIRO MMLE simulations in our analysis as this model has anomalously high Arctic Sea, meets neither of the criteria of Wang and Overland, and is a clear outlier among CMIP5 models[44].

Annual values for minimum/maximum monthly SIE are calculated from monthly SICs, with SIE defined as the areal extent of sea ice with concentrations greater than 15%. We calculate SIEs for each simulation in each large ensemble then compute the mean and variance across all of the members within each ensemble.

SIT in three models (CanESM2, CESM1-CAM5 and MPI) was saved as a grid-cell average thickness, whereas output from the two GFDL models is the average thickness over the ice-covered area of the grid cell. Monthly averaged ice-covered thickness from the GFDL models was multiplied by the monthly average SIC of each cell to get grid-cell average SIT. Monthly average SIT computed from ice-covered thickness may differ from the monthly average of daily grid-cell average thickness, particularly when there is high variability in daily SICs. We confined our analysis of relationships with monthly SIT (Fig. 3) to the Arctic Ocean (68°–90° N from 100°–243° E, and 80°–90° N elsewhere—see inset in Fig. 3) for three reasons: this region had the highest consistent correlations (for example, for each ensemble) between changes in high-latitude February surface temperatures and SIT, this region has the highest SICs in all models, which therefore reduces possible discrepancies between SIT calculations as well as reduced influence of differences in marginal seas (GFDL-CM3, for example, as extraordinarily high SIT in a few grid cells in the Canadian Archipelago) (see also ref. [74]) and this region is completely ice covered in all models at the beginning of the twenty-first century and experiences changes in thickness before changes in concentration.

The CESM1-CAM5 sea-ice model has five sub-grid-scale SIT categories (lower ice-thickness bounds of 0, 0.64, 1.39, 2.47 and 4.57 m thick, respectively) with associated output that includes ice concentrations for each of the ice-thickness categories. We are thus able to explore how SICs of different thickness categories relate to winter surface air temperature changes in that model and report this qualitatively. Other models in the MMLEA lacked this sub-grid-scale data, and so we were not able to perform a similar analysis across the remaining models.

Mean high-latitude temperature calculation. High-latitude mean temperature data for Fig. 3 and Supplementary Table 1 were computed by taking the area-weighted average of all grid cells from 70° to 90° N.

Precipitation-phase change calculation. Climate models tend to simulate too much precipitation in weaker events and too little precipitation in more-intense events[75–79], and thus estimating changes in precipitation frequency, duration and intensity from future scenarios can be complicated and beyond the scope of this paper. However, the form of precipitation—liquid or solid—is directly related to temperature, and precipitation-phase changes can have enormous environmental and societal implications (for example, refs. [60–62] and references therein). Two models in the CMIP5-MMLE (CanESM2 and CESM1-CAM5) include separate liquid and solid precipitation, enabling us to investigate changes in rain and snow seasons. We define rain or snow days as days when the total precipitation is greater than 0.2 mm d^{-1} and when 60% or more of the precipitation falls in liquid or solid form, respectively. Small differences to these thresholds do not change our results. The minimum precipitation criterion removes extremely low but non-zero precipitation events possible in simulated climate that would not be detected or measurable in the real world. First and last rain days at each grid cell are then the first and last days of the year (January 1—December 31) that qualify as rain days, respectively. The difference between the first and last rain days is defined as the duration of the rainy season.

Coding and visualization software. All analysis and figures were completed using the NCAR Command Language[80]. The scripts used to perform the analysis and generate the figures in this manuscript are available on GitHub (https://github/llandrum/NatClimCh_EmergingNewArctic/releases/tag/v1.0) and archived in Zenodo[81].

Data availability

All data used in this study are publicly available. CMIP5-MMLE output are available through the MMLEA (US CLIVAR Multi-Model LE Archive (NCAR); http://www.cesm.ucar.edu/projects/community-projects/MMLEA/). The Walsh extended and NSIDC SICs are available online (https://nsidc.org/).

Code availability

Code to produce all figures is available from the corresponding author.

References

73. Arguez, A. & Vose, R. S. The definition of the standard WMO climate normal: the key to deriving alternative climate normals. *Bull. Am. Meteorol. Soc.* https://doi.org/10.1175/2010BAMS2955.1 (2011).
74. Labe, Z., Magnusdottir, G. & Stern, H. Variability of Arctic sea ice thickness using PIOMAS and the CESM large ensemble. *J. Clim.* **31**, 3233–3247 (2018).
75. Randall, D. A. et al. in *Climate Change 2007: The Physical Science Basis* (eds Solomon, S. et al.) Ch. 8 (Cambridge Univ. Press, 2007).
76. Rosenblum, E. & Eisenman, I. Sea ice trends in climate models only accurate runs with biased global warming. *J. Clim.* **30**, 6265–6278 (2017).
77. Stroeve, J. & Notz, D. Insights on past and future sea-ice evolution from combining observations and models. *Glob. Planet. Change* **135**, 119–132 (2015).
78. Kinnard, C. M. et al. Reconstructed changes in Arctic sea ice over the past 1,450 years. *Nature* **479**, 509–512 (2011).
79. Soulé, P. T. & Knapp, P. A. A 400-year reconstruction of wintertime Arctic sea-ice extent using a high-elevation, mid-latitude tree-ring record. *Int. J. Biometeorol.* **63**, 1217–1229 (2019).
80. The NCAR Command Language v.6.6.2 (UCAR, NCAR, CISL and TDD, 2019); https://doi.org/10.5065/D6WD3XH5
81. Landrum, L. Scripts for figures and analysis for "Extremes become routine in an emerging new Arctic". *Zenodo* https://doi.org/10.5281/zenodo.3942733 (2020).
82. Walsh, J. E., Chapman, W. L., Fetterer, F. & Stewart, J. S. *Gridded Monthly Sea Ice Extent and Concentration, 1850 Onward, Version 2* (NSIDC, accessed 23 April 2020); https://doi.org/10.7265/jj4s-tq79

Acknowledgements

We acknowledge support from a grant from the NOAA Climate Program Office Grant NA15OAR4310166 and NSF Grant 1724748. We acknowledge the CESM Large Ensemble Community Project and high-performance computing support from both Yellowstone (ark:/85065/d7wd3xhc) and Cheyenne (https://doi.org/10.5065/D6RX99HX) provided by NCAR's Computational and Information Systems Laboratory, sponsored by the National Science Foundation. We thank the US National Science Foundation, National Oceanic and Atmospheric Administration, National Aeronautics and Space Administration, and Department of Energy for sponsoring the activities of the US CLIVAR Working Group on Large Ensembles. We also gratefully acknowledge all of the modelling groups listed in Table 1 for making their Large Ensemble simulations available in the Multi-Model Large Ensemble data repository.

Author contributions

L.L. and M.M.H. conceived the study. L.L. performed the analysis, created the figures and led the writing of the manuscript with contributions from M.M.H.

Competing interests

The authors declare no competing interests.

Additional information

Extended data is available for this paper at https://doi.org/10.1038/s41558-020-0892-z.

Supplementary information is available for this paper at https://doi.org/10.1038/s41558-020-0892-z.

Correspondence and requests for materials should be addressed to L.L.

Peer review information *Nature Climate Change* thanks John Walsh and the other, anonymous, reviewer(s) for their contribution to the peer review of this work.

Reprints and permissions information is available at www.nature.com/reprints.

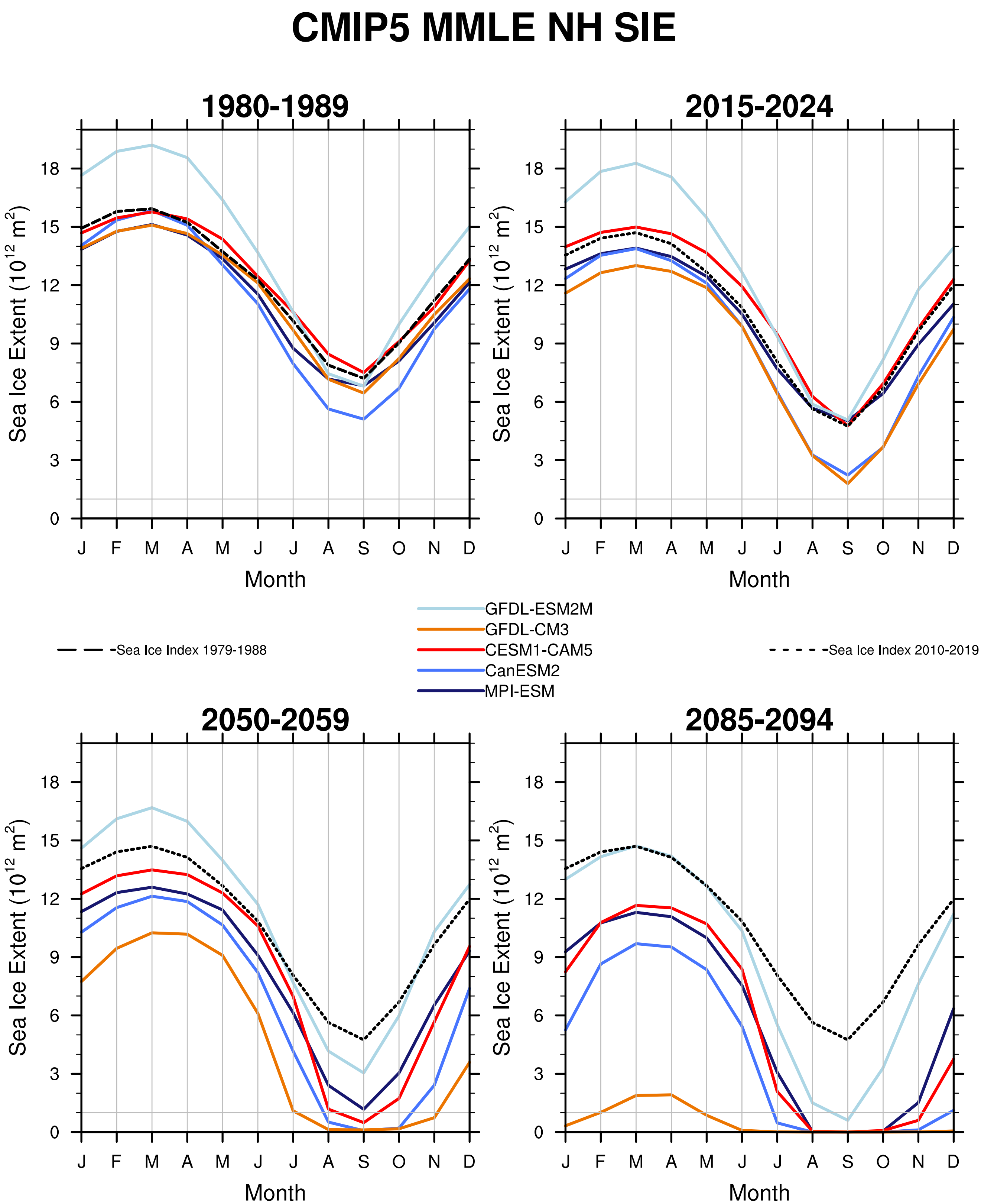

Extended Data Fig. 1 | CMIP5-MMLE NH SIE monthly climatology for 5 decades. Dashed/dotted lines indicate (1979–1988)/(2010–2019) monthly decadal averages from the NSIDC ice index[5]. Solid grey line indicates the 1 million km^2 'Ice Free' definition.

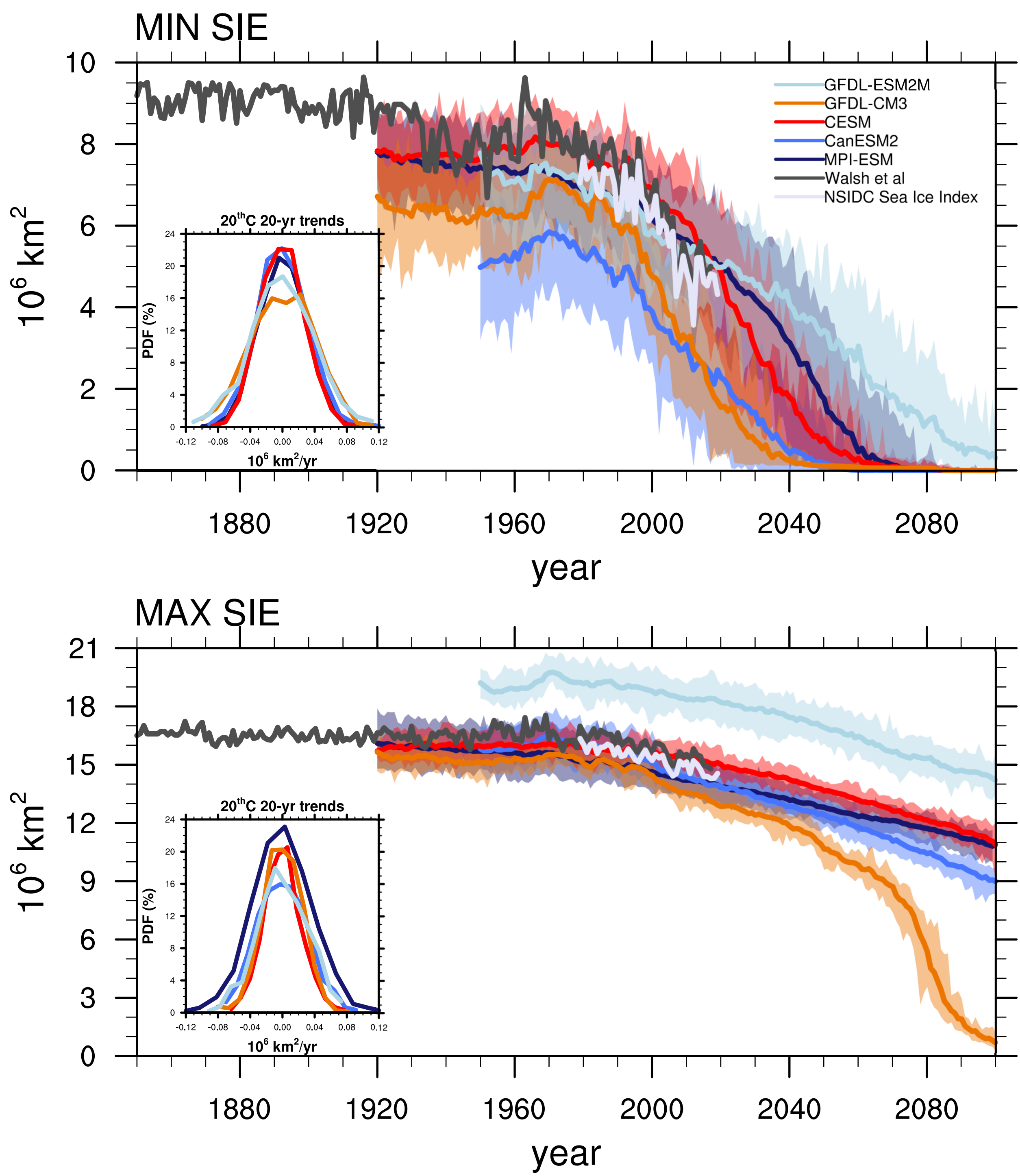

Extended Data Fig. 2 | CMIP5-MMLE and observational based Arctic Sea Ice extents. Bold solid lines indicate ensemble mean, with opaque polygon showing range of simulations for each ensemble. Extended Sea Ice dataset[82] and NSIDC ice index[5] are shown in solid dark and light grey, respectively. Insets show PDFs for running 20 yr trends over the 20th Century for each model for both minimum and maximum SIEs.

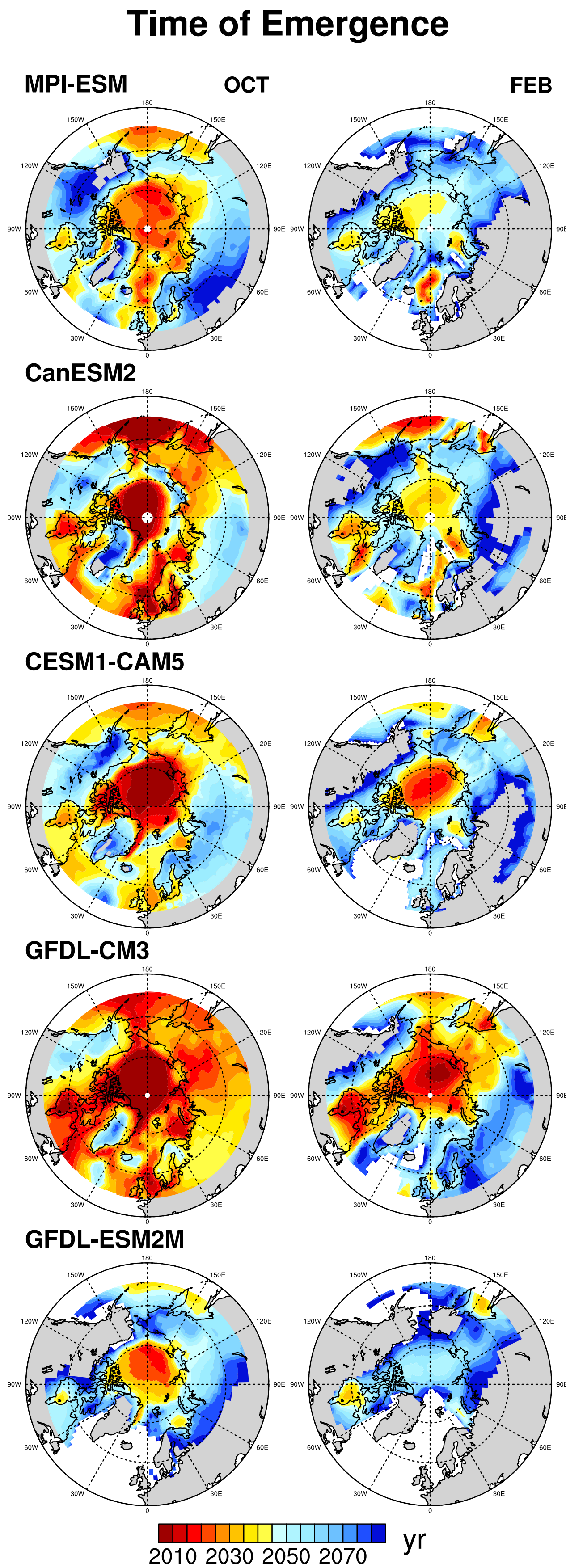

Extended Data Fig. 3 | CMIP5-MMLE Time of Emergence of monthly October and February surface air temperatures. October/February ToEs are shown in the left/right panels.

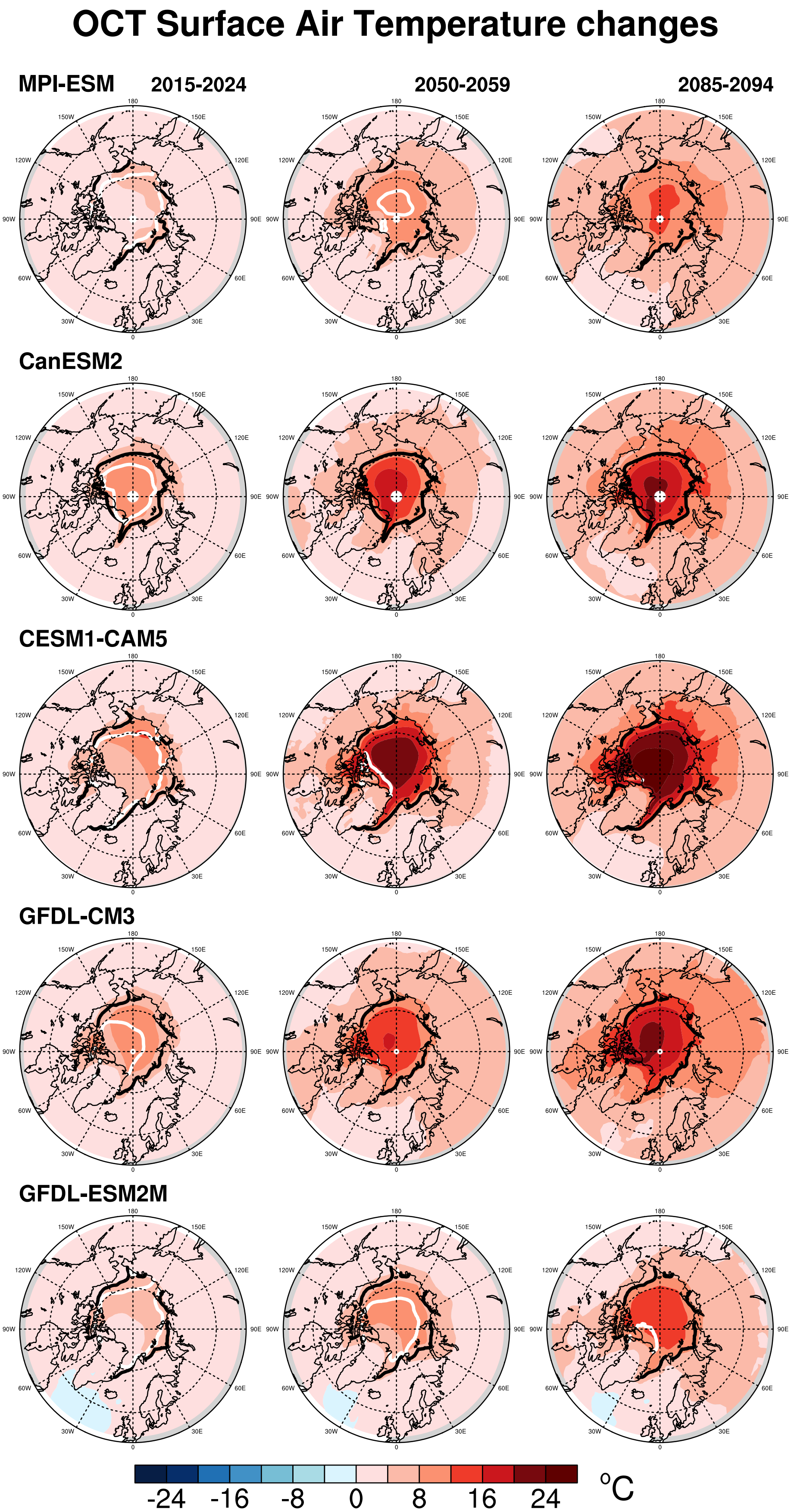

Extended Data Fig. 4 | CMIP5-MMLE mean October surface air temperature changes from (1950-1959) baseline. Results shown for early, middle and late 21st century under RCP8.5 forcing scenario. Contours indicate September 15% sea ice concentration contours for base period (1950-1959; black) and future decades (white).

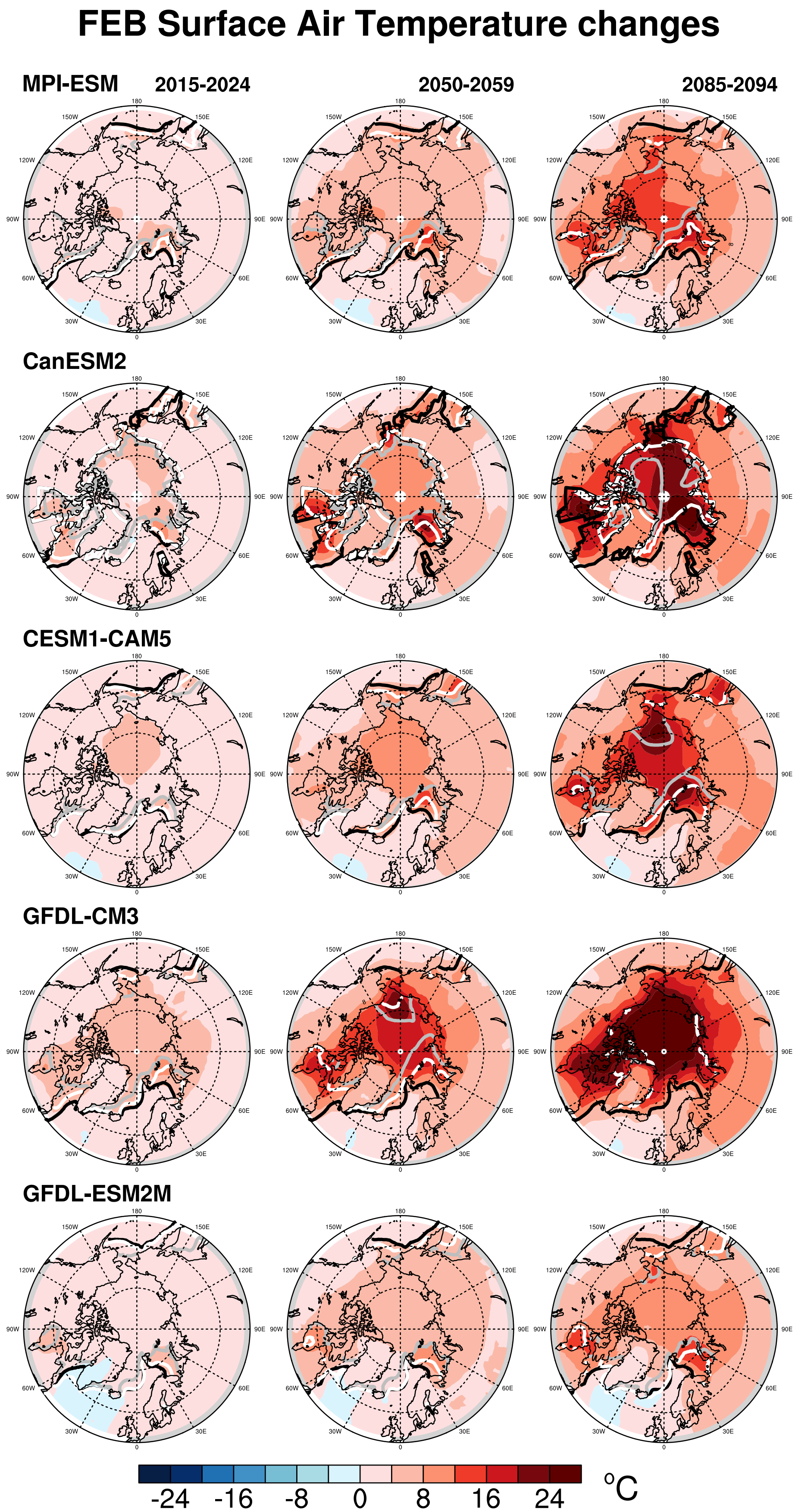

Extended Data Fig. 5 | CMIP5-MMLE mean February surface air temperature changes from (1950-1959) baseline. Results shown for early, middle and late 21st century under RCP8.5 forcing scenario. Contours indicate February 15% and 85% sea ice concentration contours for base period (1950-1959; 15% black) and future decades (15% white, 85% grey).

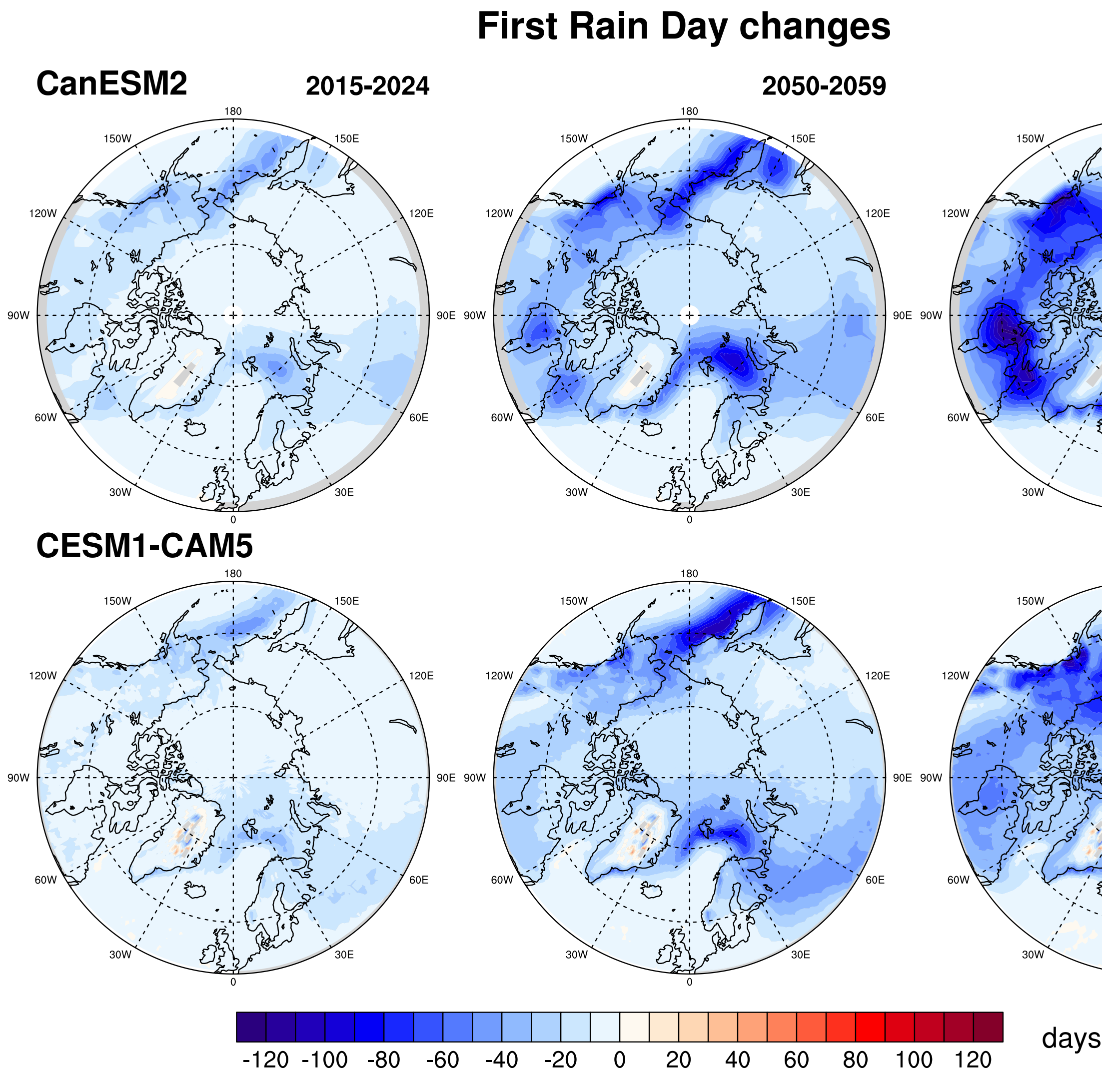

Extended Data Fig. 6 | CMIP5-MMLE first rain day changes from (1950-1959) baseline. Results shown for early, middle and late 21st century under RCP8.5 forcing scenario.

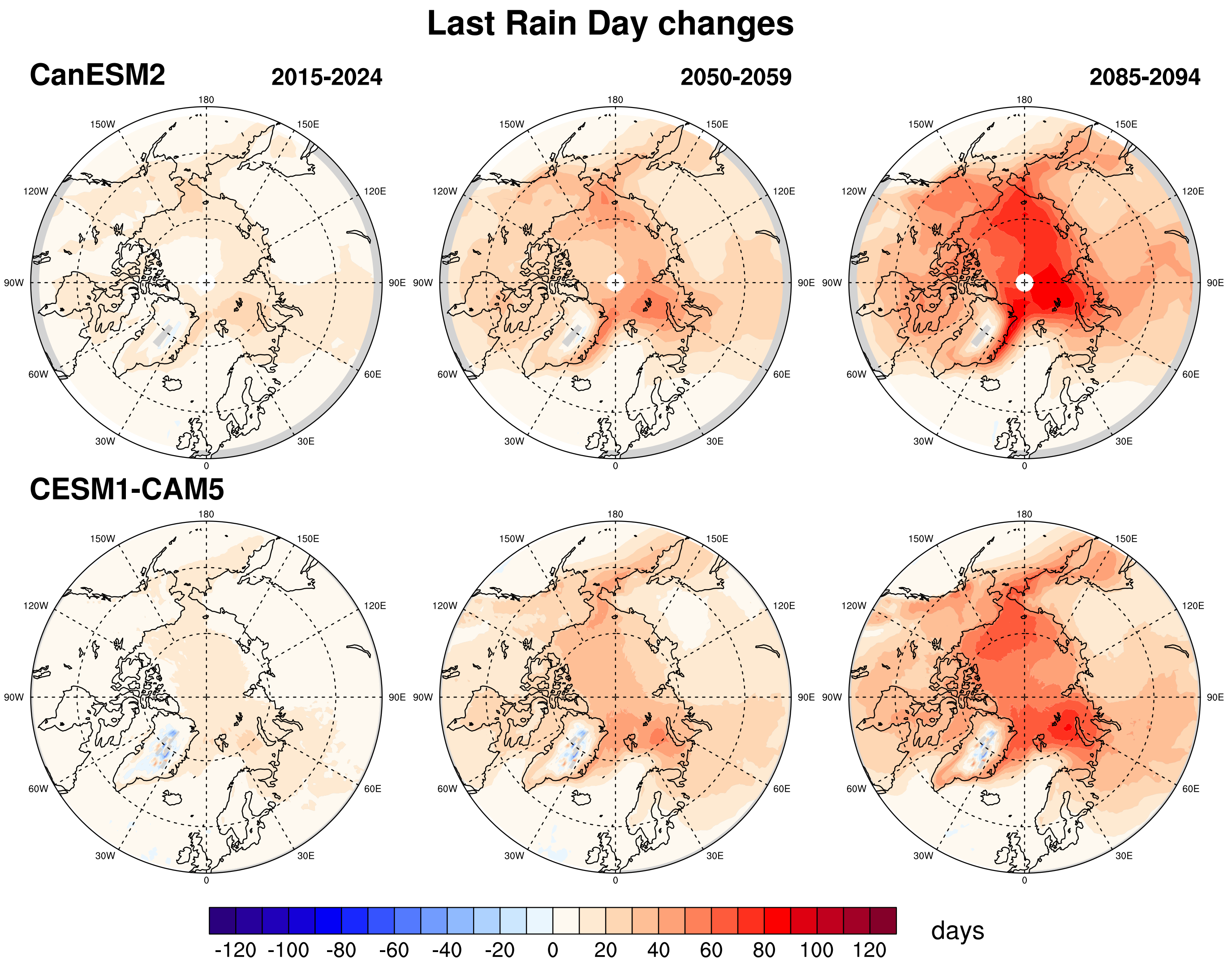

Extended Data Fig. 7 | CMIP5-MMLE last rain day changes from (1950-1959) baseline. Results shown for early, middle and late 21st century under RCP8.5 forcing scenario.

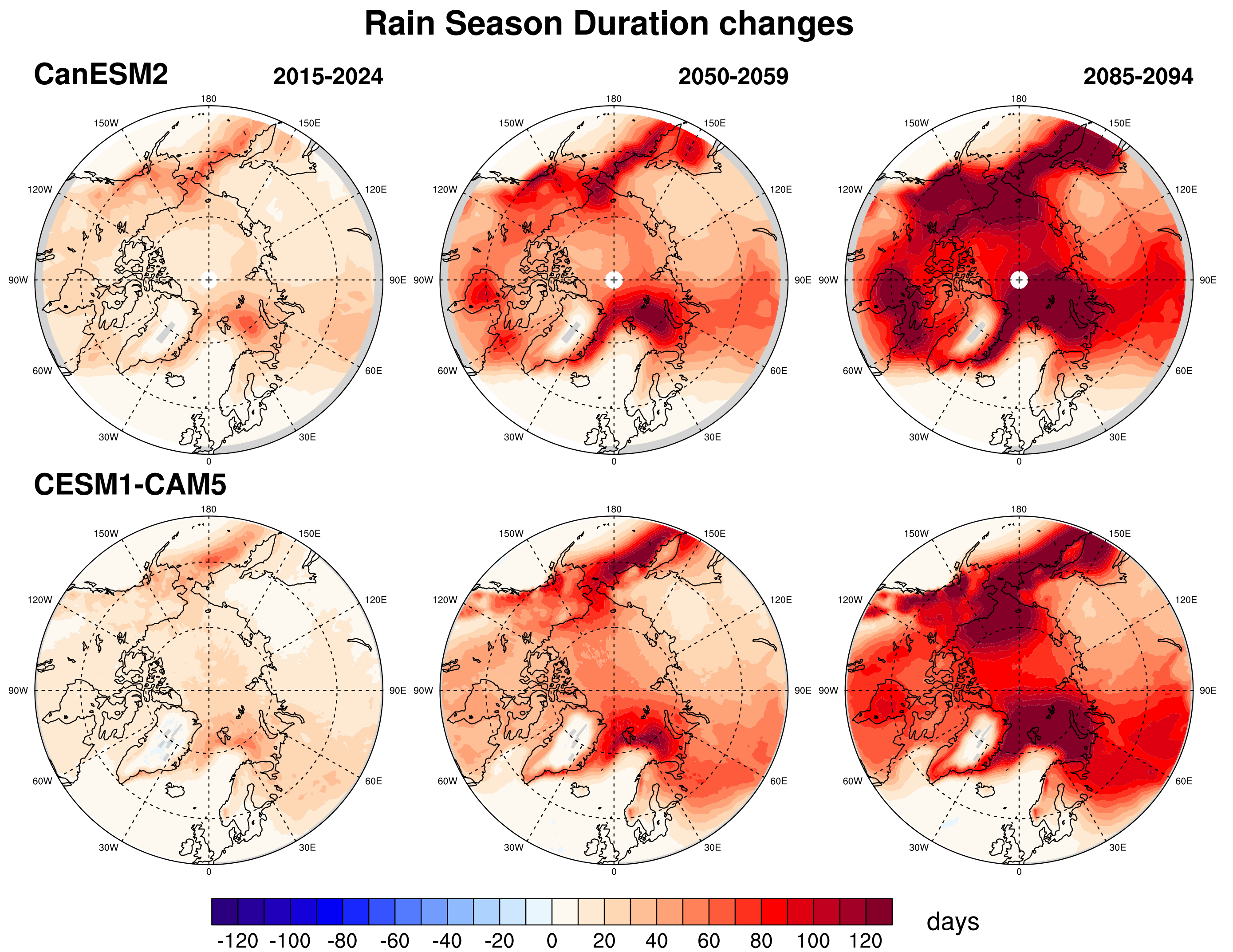

Extended Data Fig. 8 | CMIP5-MMLE rain season duration from (1950-1959) baseline. Results shown for early, middle and late 21st century under RCP8.5 forcing scenario.